BCPT Basic & Clinical Pharmacology & Toxicology

Basic & Clinical Pharmacology & Toxicology, 2013, **113**, 8–18 Doi: 10.1111/bcpt.12057

Total Synthetic Protoapigenone WYC02 Inhibits Cervical Cancer Cell Proliferation and Tumour Growth through PIK3 Signalling Pathway

Yun-Ju Chen[1,2,3], Nari Kay[2]*, Jinn-Moon Yang[4,5], Chih-Ta Lin[4], Hsueh-Ling Chang[1,3], Yang-Chang Wu[6,7,8], Chi-Feng Fu[2], Yu Chang[9], Steven Lo[10], Ming-Feng Hou[11], Yi-Chen Lee[12], Ya-Ching Hsieh[3] and Shyng-Shiou Yuan[1,2,3,13]

[1]Department of Biological Science and Technology, I-Shou University, Kaohsiung, Taiwan, [2]Department of Obstetrics and Gynecology, E-DA Hospital, Kaohsiung, Taiwan, [3]Department of Medical Research, E-DA Hospital, I-Shou University, Kaohsiung, Taiwan, [4]Institute of Bioinformatics and Systems Biology, National Chiao Tung University, Hsinchu, Taiwan, [5]Department of Biological Science and Technology, National Chiao Tung University, Hsinchu, Taiwan, [6]Graduate Institute of Integrated Medicine, College of Chinese Medicine, China Medical University, Taichung, Taiwan, [7]Natural Medicinal Products Research Center, China Medical University Hospital, Taichung, Taiwan, [8]Graduate Institute of Natural Products, College of Pharmacy, Kaohsiung Medical University, Kaohsiung, Taiwan, [9]Department of Obstetrics and Gynecology, Kaohsiung Medical University Hospital, Graduate Institute of Medicine, College of Medicine, Kaohsiung Medical University, Kaohsiung, Taiwan, [10]Department of Plastic and Reconstructive Surgery, E-DA Hospital, Kaohsiung, Taiwan, [11]Cancer Center, Kaohsiung Medical University Hospital, Kaohsiung, Taiwan, [12]Graduate Institute of Medicine, College of Medicine and Department of Anatomy, Kaohsiung Medical University, Kaohsiung, Taiwan and [13]Translational Research Center, Cancer Center and Department of Obstetrics & Gynecology, Kaohsiung Medical University Hospital, Kaohsiung Medical University, Kaohsiung, Taiwan

(Received 16 November 2012; Accepted 28 January 2013)

Abstract: Flavonoids have been intensively explored for their anticancer activity. In this study, a total synthetic flavonoid protoapigenone, known as WYC02, was analysed for its potential anticancer activity on human cervical cancer cells as well as the underlying mechanisms for these effects. The site-moiety maps are used to explore the binding site similarity, pharmacophore and docking pose similarity. The effect of WYC02 on cell viability, migration, invasion and apoptosis as well as the underlying mechanisms was analysed *in vitro* using human cervical cancer cells. The effect of WYC02 on *in vivo* tumour growth was assessed in a tumour xenograft study. WYC02 inhibited cell proliferation, MMPs activity, migration and invasion in cervical cancer cells. We speculated that WYC02 might inhibit the activities of PIK3 family proteins, including PIK3CA, PIK3CB, PIK3CD and PIK3CG. Indeed, WYC02 decreased the expression of PIK3 family proteins, especially PIK3CG, through ubiquitination and inhibited the activities of PIK3CG and PIK3 downstream molecules AKT1 and MTOR in cervical cancer cells. Furthermore, PIK3 signalling pathway was involved in the inhibitory effect of WYC02 on cervical cancer cell proliferation and tumour growth *in vitro* and *in vivo*. WYC02 inhibits cervical cancer cell proliferation and tumourigenesis via PIK3 signalling pathway and has the potential to be developed as a chemotherapeutic agent in cervical cancer.

Cervical cancer is one of the major gynaecological malignancies among women throughout the world, especially in developing countries [1]. Conventional therapies for cervical cancer include surgery, radiotherapy and chemotherapy [2]. For locally advanced cervical cancer, neoadjuvant chemotherapy (NACT) before surgery or during radiotherapy is an accepted primary treatment, with the ability of NACT to reduce tumour size, radiosensitize tumours and to improve disease control by decreasing the repair of cancer cell damage caused by radiation [3,4]. The most commonly used chemotherapy regimen in cervical cancer is platinum-based chemotherapy that can significantly reduce local treatment failure and improve overall disease-free survival [5,6]. However, resistance to platinum-based chemotherapy is relatively common [7], and therefore, development of new chemotherapeutic agents is required.

The application of naturally existing dietary regimens in cancer prevention has been well reported [8,9] and among these natural diet regimens, flavonoids have been intensely studied in recent years. Flavonoids are polyphenolic, secondary metabolites with broad-spectrum pharmacological activities and have various biological effects, including induction of cytotoxicity, apoptosis and antiproliferation [2,10]. Some flavonoids, for example, LYG-202, N101-2, nobiletin and hispidulin, have been shown to inhibit angiogenesis and cell growth of cervical, gastric and pancreatic cancers through phosphatidylinositol 3-kinase (PIK3)/AKT1 signalling [11–14]. Activation of class I PIK3s is one of the most important signal transduction pathways used by cell-surface receptors to control intracellular events, known to be involved in the regulation of cell growth, survival, proliferation, movement and inflammation [15–18]. There are four isoforms of the catalytic subunit of class I PIK3s: PIK3CA, PIK3CB, PIK3CD and

Authors for correspondence: Shyng-Shiou Yuan, Department of Obstetrics and Gynecology, E-DA Hospital, No.1, E-DA Road, Yan-Chau District, Kaohsiung 824, Taiwan (fax +886 7 6155352, e-mail yuanssf@ms33.hinet.net).
Ya-Ching Hsieh, Department of Medical Research, E-Da Hospital, I-Shou University, No. 6, Yi-Da Road, Yan-Chau District, Kaohsiung 824, Taiwan (fax +886 7 6150945, e-mail: yaching.hsieh@gmail.com).
*Co-first author.

PIK3CG [15,16]. Presently, class I PIK3 signalling pathway is emerging as an exciting new area for the development of novel therapeutic strategies.

Recently developed drug design models, based on structure–activity relationship and pharmacological interaction, have been used to explore the ligand-binding possibility of a therapeutic target. Most current virtual screening (SV) methods employ flexible docking tools, such as incremental and fragment-based approaches (DOCK and FlexX) and evolutionary algorithms (GOLD, AutoDock and GEMDOCK), to identify lead compounds for the target proteins [19–21]. These methods apply the pharmacological interaction preferences to select the ligands that form pharmacological interactions with target proteins and use the ligand preferences to eliminate the ligands that violate electrostatic or hydrophilic constraints. Recently, an innovative technology *i*GEMDOCK has been developed to facilitate steps from preparation of target proteins and ligand libraries towards post-screening analysis [22]. iGEMDOCK is especially useful for post-screening analysis and inferring pharmacological interactions from screening compounds. When the structure of the target protein is known, receptor-based computational methods can be employed. In a previous study, we applied virtual molecule docking to discover the pharmacological interactions on three therapeutic protein targets, including oestrogen receptor α for antagonists and agonists [23]. Our results also revealed that the derived pharmacological interactions are often essential for ligand binding or maintaining biological functions of these targets.

In our initial screening, the total synthetic protoapigenone WYC02 contains cytotoxic activity against human cancer cells *in vitro* [24]. In this study, the virtual screening (SV) method that employed flexible docking tools was first applied to isolate candidate cellular targets of WYC02, followed by *in vitro* and *in vivo* studies to further clarify potential anticancer activity and the underlying mechanisms against cervical cancer cells.

Materials and Methods

Origins of total synthetic protoapigenone WYC02. The plant-derived natural flavonoid protoapigenone was first isolated from *Thelypteris torresiana* (Gaud.), followed by total synthesis and renamed WYC02 [24].

Cell culture. HeLa cervical adenocarcinoma and SiHa cervical sarcoma cell lines used in this study were cultured according to the instructions from American Type Culture Collection (ATCC, Manassas, VA, USA). The genotypes and phenotypes of the cell lines were authenticated by Bioresource Collection and Research Centre (Hsinchu, Taiwan). Cells were grown in DMEM medium (Invitrogen, Carlsband, CA, USA), supplemented with 10% foetal bovine serum (Hyclone, Logan, UT) and antibiotics (100 units/mL penicillin, 100 μg/mL streptomycin and 2.5 μg/mL amphotericin B) (Biological Industries, Haemek, Israel).

Colony formation assay. To determine long-term effects of WYC02 on cell proliferation, HeLa cells were treated with WYC02 for 3 hr. The detailed colony formation assay procedure followed the previous report [25].

Cell cycle analysis. Fluorescence-activated cell sorting (FACS) analysis was applied to analyse the cell cycle distribution. In brief, HeLa cells were treated with WYC02 for 24 hr and FACS analysis was performed according to a previous article [26].

Immunoblotting. Immunoblotting was performed according to a previous article [26]. Antibodies against CDC25A and P-RB1(Thr356) were obtained from Santa Cruz Biotechnology (Santa Cruz, CA, USA). RB1, ACTB, PIK3CA, PIK3CB, PIK3CD, PIK3CG, P-AKT1 (Thr308and Ser473), AKT1, ubiquitin and Flag were obtained from Genetex (Irvin, CA, USA). P-CDC25C(Ser216), P-CDC2(Thr161), cleaved CASP8, cleaved CASP9, cleaved CASP3, cleaved PARP1, P-MTOR(Ser2448) and MTOR were obtained from Cell signalling Technology (Beverly, MA, USA). P-PIK3CG(Ser1100) was obtained from Abgent (San Diego, CA, USA).

Annexin V apoptosis assay. Annexin V-FITC fluorescence microscopy kit (BD Biosciences, San Jose, CA, USA) was used to detect early apoptotic cells during apoptotic progression. HeLa cells on chamber slides were treated with 10 μM WYC02 for 3 hr, annexin V apoptosis assay was performed according to a previous article [27].

Terminal Deoxynucleotidyl Transferase dUTP Nick-End Labelling Assay. HeLa cells were treated with 10 μM WYC02 for 24 hr and then stained for determination of apoptotic cells using the DeadEnd Colorimetric TUNEL system (Promega, Madison, WI, USA). Terminal Deoxynucleotidyl Transferase dUTP Nick-End Labelling (TUNEL) assay was performed according to a previous article [27].

Wound-healing assay. About 1×10^5 HeLa cells were seeded in 12-well plates and allowed to reach 100% confluence. Cell monolayer was scratched with 200-μL pipette tip of constant width. Cells were then treated with WYC02 for 48 hr. and wound-healing assay was performed according to a previous article [28].

Transwell invasion assay. About 7×10^3 HeLa cells were seeded on 8-μm-pore ECM-coated insert chamber (Corning, NY, USA) and allowed to reach 100% confluence. Cells were treated with WYC02 for 48 hr, and invasion assay was performed according to a previous article [29].

Gelatin zymography analysis. Gelatin zymography is mainly used for the detection of gelatinase activity. 5×10^4 HeLa cells were plated in 24-well plates and allowed to reach 100% confluence. Cells were treated with WYC02 for 48 hr, and gelatin zymography analysis was performed according to a previous article [30].

Protein sequence analysis and molecular modelling. We obtained protein sequences of PIK3 catalytic subunits from GenBank and aligned them using the default settings with ClustalW2. The docking of WYC02 into the binding site of the PIK3 catalytic subunits was explored using iGEMDOCK software [24]. The 3D structure of WYC02 was prepared by DS ViewerPro 6.0 from Accelrys, and the structures of the quercetin and ATP were extracted from the PIK3CG crystal structures (PDB code 1E8W and 1E8X, respectively) in the Protein Data Bank (PDB). Homology modelling of HsPIK3CB and HsPIK3CD was done using Swiss-Model with 2Y3A and 2WXJ of crystal structures in the PDB as templates. The binding pockets of the HsPIK3CA (PDB code 3HHM), HsPIK3CB (PDB code 2Y3A), HsPIK3CD (PDB code 2WXP) and HsPIK3CG (PDB code 3DBS) were defined to include the residues within an 8Å radius sphere centred around the binding site of their ligands. The coordinates of the atoms in the binding pockets were obtained from the PDB. The interaction profile was performed with dChip, and the algorithm of

hierarchical clustering centroid linkage was employed. The site-moiety map analyses of PIK3 catalytic subunits were performed with SiMMap.

Reverse transcription polymerase chain reaction. Reverse transcription polymerase chain reaction (RT-PCR) was analysed with One-s RT-PCR kit (QIAGEN, Foster, CA, USA). Specific cDNA for the PIK3CG and glyceraldehyde-3-phosphate dehydrogenase (GAPDH) were amplified with primer pairs (PIK3CG: 5′-GCTTGA AAACCTGCAGAATTCTCAAC-3′ and 5′-CGTCTTTCACAATCTC GATCATTCC-3′; GAPDH: 5′-TGATGACATCAAGAAGGTGGTG AAG-3′ and 5′-TCCTTGGAGGCCATGTGGGCCAT-3′) by PCR, which were performed according to a previous article [31].

Immunoprecipitation. Cells were re-suspended in lysis buffer (Millipore Corporation, Billerica, MA, USA). 50 μg cell lysates served as input control and 1.2 mg cell lysates were incubated with 3 μg of PIK3CG antibody at 4°C overnight. To study the ubiquitination of PIK3CG, immunoprecipitation was performed by Catch and Release v2.0 reversible immunoprecipitation system (Millipore Corporation).

Ex vivo tumour xenograft study. All experiments using mice were performed according to the guidelines of the Animal Committee and with ethics approval from the institutional review board of E-Da Hospital/I-Shou University (Approval No.: IACUC-ISU-96024). Six-week-old female immunodeficient (Foxnlnu/Foxnlnu) mice were injected subcutaneously with 5×10^6 HeLa cells at the right flank. When tumours became visible (approximately an average diameter of 3 mm), mice were treated intraperitoneally with WYC02 at 1.09 μg/g (a dose equals to the IC_{50}) body-weight or vehicle (PBS) every 2 days. Tumour volumes were calculated according to a standard formula: $width^2 \times length/2$ and performed according to a previous article [27].

Immunohistochemistry. Immunohistochemistry protocol was followed accordingly to a previous report [32]. Tissue sections were incubated overnight at 4°C with 100X diluted of PIK3CA, PIK3CB, PIK3CG or PIK3CD antibodies, which were obtained from Genetex.

Transfection of PIK3CG plasmid DNA. HeLa cells were transfected for 16 hr with human PIK3CG expression plasmid or empty vector, purchased from Addgene (Cambridge, MA, USA; Cat#20574) using Lipofectamine 2000 according to Invitrogen's respective protocol (Invitrogen). After removal of transfection medium, the cells were incubated with fresh medium for 48 hr and then selected for neomycin-resistant cells using 500 μg/mL neomycin (A.G. Scientific, San Diego, CA, USA) for 7 days.

Transfection of PIK3CG siRNA. HeLa cells were seeded at 5×10^3 cells per well in a 96-well dish. At 20 hr after seeding, the cells were transfected with human PIK3CG siRNA-SMARTpool (Dharmacon, Lafayette, CO, USA, Cat# DAMD-005274-02) (Target sequences: CUACAGCCCUAUCAAAUGA, GGUCCAGGCUGUGAAAUUU, AGAAAUCUCUGAUGGAUAU, GACGUCAGUUCCCAAGUUA) or non-target siRNA Pool (Dharmacon, Cat# DAMD-001206-13) using DharmaFECT1 transfection reagent (Dharmacon Cat# DAMD-2001-02). Briefly, 4 μL of DharmaFECT1 was diluted in 196 μl of serum-free medium and was incubated at room temperature for 5 min. In a separate sterile tube, 10 μL of siRNA oligos (5 μM stock) was mixed with 190 μL of serum-free medium and incubated at room temperature for 5 min. The diluted DharmaFECT1 and diluted siRNA oligos were then mixed together and incubated at room temperature for another 20 min. At the end of the incubation period, 1.6 mL of complete growth medium was added to the mixture, and 100 μL of this final mixture was dispensed to each of the 96 wells for 16 hr. After removal of transfection medium, the cells were incubated with fresh medium for 48 hr and then treated WYC02 for 48 hr.

Statistical analysis. Quantitative data are presented as mean ± S.E.M. The statistical significance among three or more groups was analysed by one-way analysis of variance (ANOVA) and Duncan's test. Two-sided Student's *t*-test was used to determine the significance between two groups. $p < 0.05$ was considered statistically significant.

Results

Total synthetic protoapigenone WYC02 inhibited cervical cancer cell viability.

The cytotoxicity of WYC02 on human cervical cancer cells was first analysed in this study. WYC02 was toxic to the three tested cell lines HeLa, C33A and SiHa [inhibitory concentration (IC_{50}) = 4.23 μM, 5.37 μM and 8.12 μM, respectively]. WYC02 had higher cytotoxic activity against HeLa cells than the clinically used drug cisplatin at 48 hr of treatment (IC_{50} = 4.23 μM and 11.80 μM, respectively). The effect of WYC02 on cell colony formation and cell cycle distribution was further analysed. WYC02 treatment significantly inhibited HeLa cell clonogenicity (fig. 1A). WYC02 treatment accumulated HeLa cells at S and G2/M phases in a dose-dependent manner (fig. 1B). In agreement with cell cycle distribution, an increased phosphorylation of G1-S regulator RB1 and the decreased levels of G2/M regulators CDC25A and P-CDC2 were observed in HeLa cells after WYC02 treatment (fig. 1C).

WYC02-induced apoptotic cell death in cervical cancer cells.

To study the effects of WYC02 on cell apoptosis, annexin V (marker of early apoptosis) assay and TUNEL (marker of late apoptosis) assay were applied. A significant increase in annexin V and TUNEL positive cells were observed in HeLa cells after 10 μM WYC02 treatment (figs 1D,E). Further study by immunoblotting analysis demonstrated that WYC02 treatment induced a dose-dependent cleavage CASP8, CASP9, CASP3 and PARP1 in HeLa cells (fig. 1F).

WYC02 decreased MMPs activities and inhibited migration/invasion in cervical cancer cells.

A critical event in cancer cell migration and invasion is the degradation of extracellular matrix (ECM), while the expression of matrix metalloproteinases (MMPs) is necessary for ECM degradation [33]. MMP-2 (gelatinase A) and MMP-9 (gelatinase B) are able to degrade most of the ECM components and are the major MMPs secreted from HeLa cells [34]. In this study, we found that WYC02 decreased the efficiency of cell migration, invasion, activities of MMP-2 and MMP-9 in HeLa cells in a dose-dependent manner (fig. 2). However, no significant cytotoxicity was observed in 100% confluent HeLa cells when treated with 2 μM WYC02 for 48 hr [(IC_{50}) = 10.79 μM for HeLa cells] (fig. S1).

WYC02 has inhibitory potential on PI3K catalytic subunits.

To explore the target proteins, especially kinases, for WYC02 activity, ligand similarity was applied. We speculated that

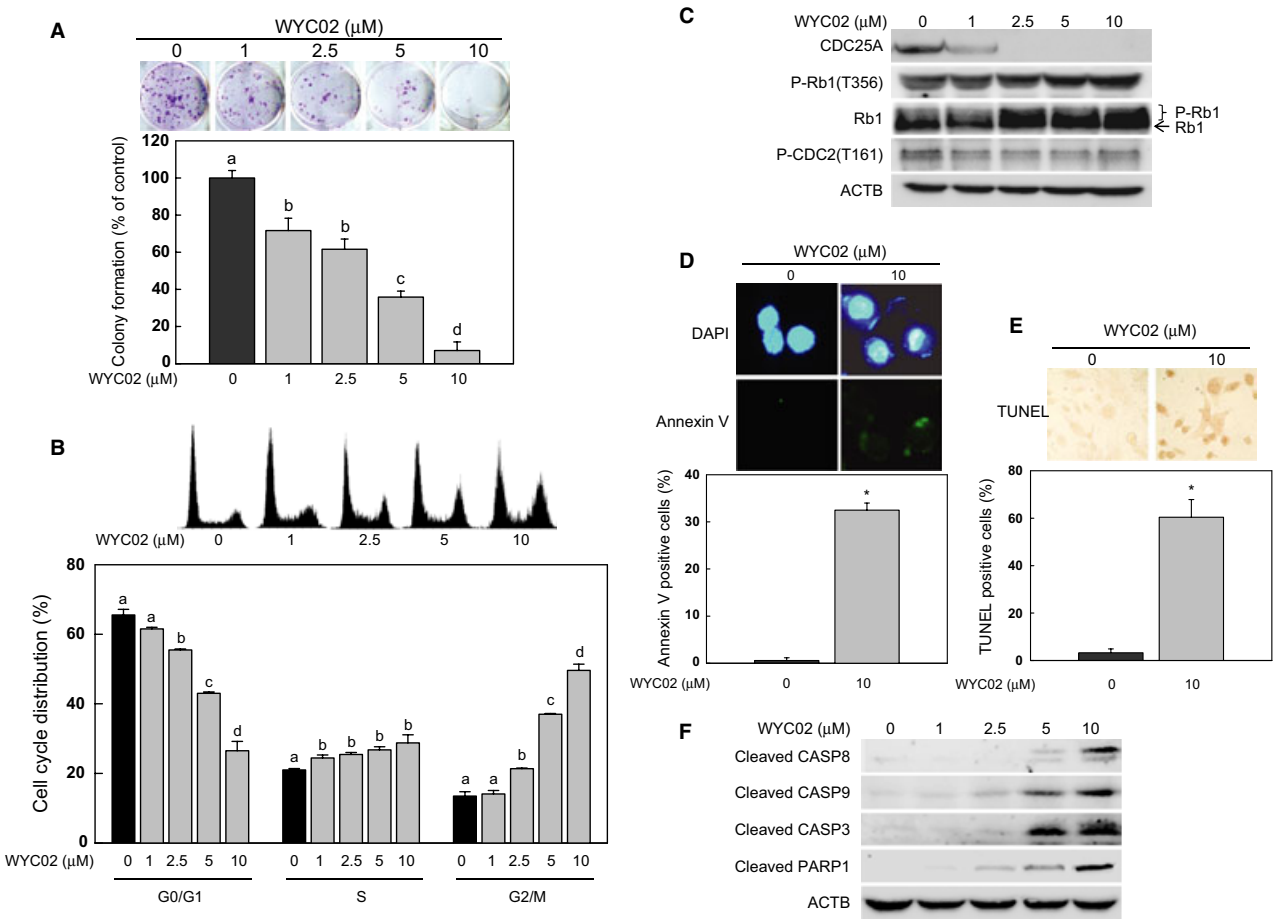

Fig. 1. WYC02 decreased cell viability and induced apoptosis in HeLa cervical cancer cells. (A) and (B) HeLa cells after treatment with vehicle control or WYC02 were analysed for colony formation and cell cycle distribution by flow cytometry. (C) Immunoblotting analysis of the expression of cell cycle regulatory proteins in HeLa cells at 24 hr after WYC02 treatment. (D and E) HeLa cells treated with 10 μM WYC02 were analysed by annexin V and TUNEL assay. (F) Immunoblotting analysis of the expression of apoptosis-related proteins at 24 hr after WYC02 treatment. Each bar represents the mean ± S.E.M. *Indicates a significant difference ($p < 0.05$) when compared with the vehicle control without WYC02.

WYC02 had inhibitory effects on PIK3 catalytic subunits, based on the results of sequence conservation of key interacting residues among PIK3 catalytic subunits, WYC02 docked conformations of PIK3 catalytic subunits, interaction profile of known PIK3 catalytic subunit general inhibitors and site-moiety map analysis of PIK3 catalytic subunits. To further analyse the inhibition mechanisms of PIK3 catalytic subunit general inhibitors on PIK3 catalytic subunits, key interactions were extracted from the cocrystal structures of ATP and PIK3 catalytic subunit general inhibitors to PIK3 catalytic subunits, and the binding sites of PIK3 catalytic subunits were divided into several motifs and regions, including P-loop, hinge, catalytic loop (C-loop), activation loop (A-loop), adenine pocket (AP), hydrophobic region I and II (HI and HII), phosphate-binding region (PB), specific pocket (SP), ribose-binding region (RB) (fig. 3A). All PIK3 catalytic subunit general inhibitors form hydrogen bonds with hinge, hydrophobic region I and phosphate-binding region, and hydrophobic interactions with adenine pocket, hydrophobic region I, phosphate-binding region and specific pocket among PIK3 catalytic subunits and compete with ATP by targeting ATP-binding site (fig. 3B). According to the hierarchical cluster (C2) of interaction profile, similar inhibitors of PIK3 catalytic subunits have a similar interaction profile. In addition, WYC02 docked conformations of PIK3 catalytic subunits (C1) showed a similar interaction profile to PIK3CG inhibitor (IC_{50} = 3.8 μM, K_d = 0.28 μM), QUE, quercetin, a similar flavonoid to WYC02 (fig. 3B).

The sequences of PIK3 catalytic subunits are highly conserved, especially in interacting residues of ATP and PIK3 catalytic subunit general inhibitors to PIK3 catalytic subunits, catalytic residues of PIK3 catalytic subunits (fig. 3C). The similarities of PIK3 catalytic subunits are not only shown in sequences, but also presented in binding environments. The site-moiety map analysis showed that PIK3 catalytic subunits are highly similar in anchors, interacting residue compositions and moiety preferences of each anchor (fig. 3D). All PIK3 catalytic subunits have five consensus anchors, three H-bond interacting anchors and two van der Waals interacting anchors. The consensus anchors also consist of conserved interacting residues. In moiety preference, all H-bond interacting anchors of PIK3 catalytic subunits prefer to form H-bond with oxygen atoms, including hydroxyl moiety and carbonyl moiety. All

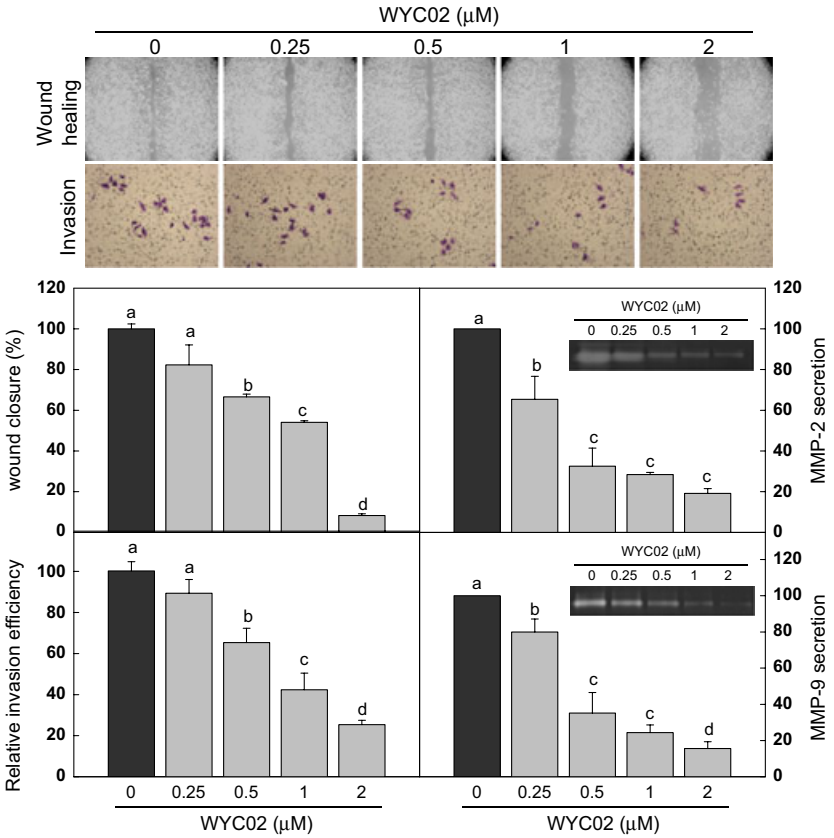

Fig. 2. WYC02 decreased HeLa cell migration, invasion and MMPs activities. HeLa cells were treated with WYC02 at various doses and the migration and invasion efficiencies were determined by wound-healing assay and ECM-coated transwell system. MMP-2 and MMP-9 activities were measured using gelatin zymography analysis. All data are shown as mean ± S.E.M.

van der Waals interacting anchors of PIK3 catalytic subunits prefer to form hydrophobic interactions with aromatic moiety. Most PIK3 catalytic subunit general inhibitors agree with these five anchors. In addition, WYC02 docked conformations of PIK3 catalytic subunits have common anchors, H1 (corresponding to hinge), V1 (corresponding to adenine pocket) and V2 (corresponding to hydrophobic region I). Furthermore, WYC02 docked conformations of PIK3CA, PIK3CB and PIK3CG target H2 anchor (corresponding to phosphate-binding region); WYC02 docked conformations of PIK3CB and PIK3CD target H3 anchor (corresponding to hydrophobic region I). All WYC02 docked conformations of PIK3 catalytic subunits target ATP-binding site, consistent with other PIK3 catalytic subunit general inhibitors, especially in a similar inhibitor, quercetin. Therefore, according to the WYC02 docked conformations, the interaction profile of PIK3 catalytic subunit general inhibitors, key interacting residue/motif conservation of PIK3 catalytic subunits and binding environments of PIK3 catalytic subunits, we believe that WYC02 has inhibitory potential effects on PIK3 catalytic subunits.

WYC02-inactivated PIK3/AKT1 signalling pathway in cervical cancer cells.

From the results of site-moiety maps for exploration of the binding site similarity, pharmacophore and docking pose similarity, we speculated that WYC02 might inhibit the activities of PIK3 family proteins including PIK3CA, PIK3CB, PIK3CG and PIK3CD. Further literature search also revealed that flavonoids suppressed cell proliferation in leukaemia cells, gastric

Fig. 3. Inhibitory potential effects of WYC02 on PI3K catalytic subunits. (A) Schematic representation of a PIK3 protein kinase ATP-binding pocket. (B) Interaction profile of PIK3 inhibitor complexes and docked conformations of WYC02 in PIK3 catalytic subunits. (C) The sequence conservation of key interacting residues among four PIK3 catalytic subunits. The catalytic residues are coloured in yellow. The key interacting residues of ATP and general inhibitors of PIK3 catalytic subunit are circled and coloured in grey, respectively. (D) Chemical structure of WYC02 and site-moiety map analysis of PIK3 catalytic subunits. The key interacting residues of ATP and general inhibitors of PIK3 catalytic subunit in the table are shown in bold and coloured in grey, respectively. The interacting residues of each anchor are labelled and the hydrogen bonds (dash with green line) between WYC02 (blue) and the PIK3 catalytic subunits (grey) are indicated. The ATP (orange) and QUE (pink) were extracted from the PIK3CG crystal structures (PDB code 1E8W and 1E8X, respectively) as the reference. The interacting anchors of H-bond and van der Waals are shown in green and grey, respectively. The figures were drawn using PyMOL software.

adenocarcinoma cells and lung cancer cells, through inhibition of PIK3/AKT1 signalling cascades [14,35,36]. Therefore, immunoblotting analysis was applied to confirm the suppressive effect of WYC02 on PIK3 family proteins. The results were consistent with the data of site-moiety maps showing that WYC02 inhibited the expression of PIK3CA, PIK3CB,

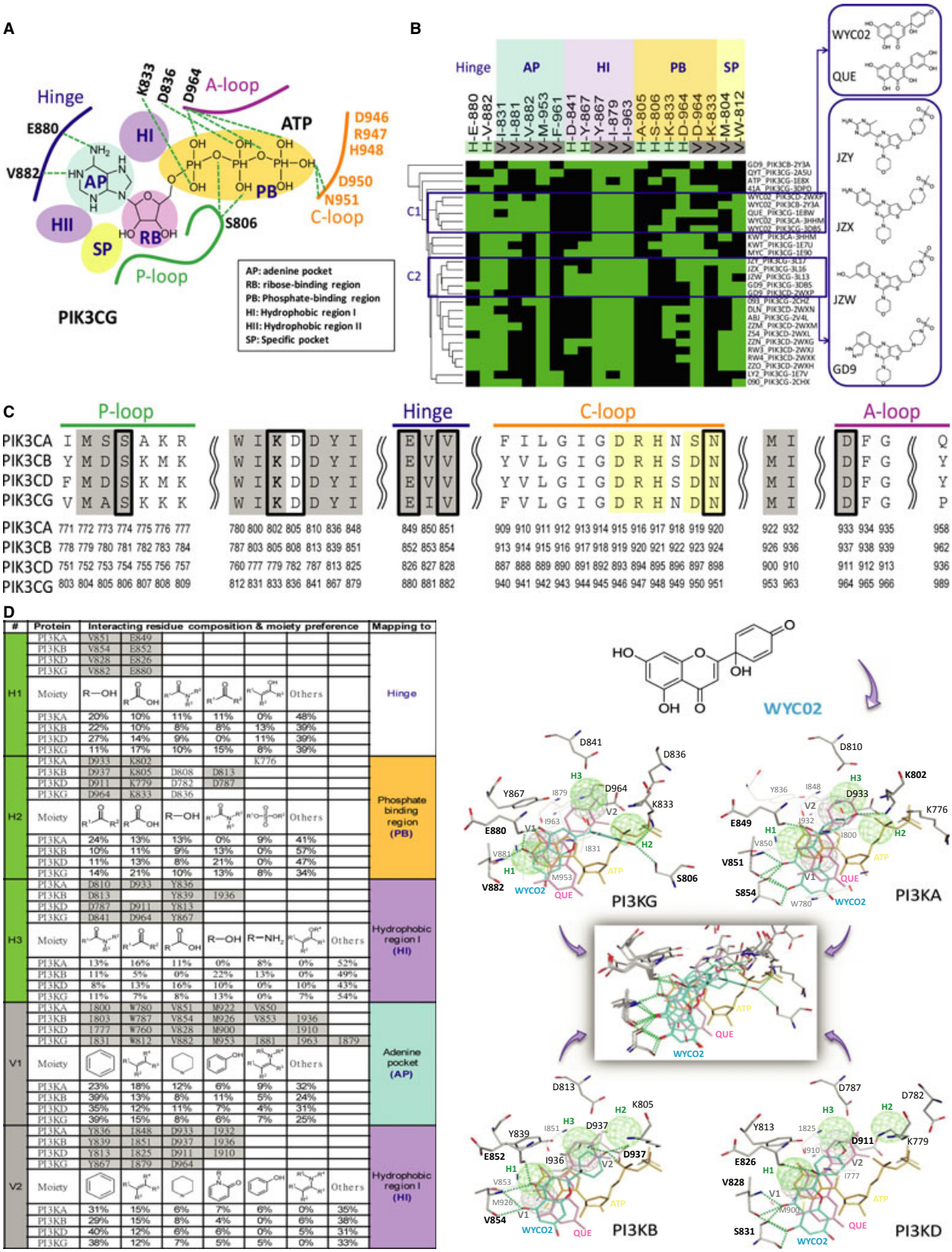

PIK3CG and PIK3CD, with the most significant suppressive effect on PIK3CG (fig. 4A). WYC02 also showed inhibitory effects on phosphorylation and activity of PIK3CG (fig. 4B). We further examined the effect of WYC02 treatment on the major downstream signalling mediators of PIK3, namely AKT1 and MTOR, in HeLa cells. Both AKT1 and MTOR kinases play important roles in cell survival [37]. Upon WYC02 treatment, the phosphorylation of AKT1 and MTOR, but not the total expression levels of AKT1 and MTOR, was suppressed (fig. 4B). These results confirmed that WYC02 decreased PIK3 expression and inactivated PIK3 signalling cascades in human cervical cancer cells.

Several mechanisms are well known to negatively regulate kinase activity, including reduction in mRNA level and induction of protein degradation [38], and PIK3 can be degraded through ubiquitination/proteasome pathway [39,40]. In this study, the RNA levels of PI3KCG were not changed in HeLa cells upon WYC02 treatment, determined by RT-PCR (fig. 4C). On the other hand, we observed that MG132, an inhibitor of proteasomal protease activity, reversed WYC02-induced decrease in PI3KCG protein level, suggesting the decrease in PI3KCA expression upon WYC02 treatment was caused by protein degradation (fig. 4D). We further tested the possibility that WYC02-induced PIK3CA degradation in HeLa cells was caused by protein ubiquitination. Upon WYC02 treatment in HeLa cells, PIK3CG coimmunoprecipitated with ubiquitin, indicating a physical interaction between the two proteins. Ubiquitination of PIK3CG was increased in HeLa cells upon WYC02 treatment (fig. 4E) and resulted in a decreased amount of PIK3CG protein (figs. 4A,D). To further analyse the involvement of PIK3CG in WYC02-induced cytotoxicity, PIK3CG-Flag was over-expressed in HeLa cells followed by cell viability analysis upon WYC02 treatment. A statistically significant reverse in cell viability was observed in PIK3CG-Flag-overexpressing HeLa cells compared with vector control cells (fig. 5A). Furthermore, PIK3CG levels were significantly reduced by siRNA knockdown, and the reduction in PI3KCG expression resulted in a significant decrease in HeLa cell viability but blocked the cytotoxicity caused by WYC02 treatment (fig. 5B).

WYC02 decreased the expression of PI3K subunits and suppressed xenograft tumour growth in nude mice.

To determine the suppressive effect of WYC02 on cervical cancer cell growth *in vivo*, nude mice xenograft model was applied. The tumour growth was significantly suppressed in the WYC02-treated group (fig. 6A). There was also no significant alteration of body-weight, haematopoiesis, liver function, renal function and organ histology in the WYC02-treated group (fig. 6B, fig. S1 and table S1). Moreover, the expression of PIK3 catalytic subunits, PIK3CA, PIK3CB, PIK3CD and PIK3CG, in xenograft tumours was decreased in WYC02-treated tumour tissues. This result confirmed that WYC02 decreased the expression of PIK3CA, PIK3CB, PIK3CD and PIK3CG in cervical cancer cells both *in vitro* and *in vivo* (fig. 4A and fig. S2).

Discussion

Virtual screening of the candidate anticancer compound WYC02.

Exploring the potential antiproliferative effects of phytochemicals, such as vinblastine and adriamycin, may open new avenues in anticancer drug design [41]. One such phytochemical, flavonoids (a subclass of polyphenols), has been previously explored in cancer therapy in their ability to suppress cancer cell proliferation, induce cell cycle arrest and promote apoptosis [10,35,42]. The present study investigated the inhibitory effect of the candidate synthetic flavonoid protoapigenone WYC02, on HeLa cell proliferation, cell cycle progression, migration, invasion, as well as an apoptosis-promoting effect. Nonetheless, thousands of mechanisms may underlie these therapeutic effects, and virtual screening was therefore employed as an efficient route to reduce the complexity of identifying potential therapeutic targets and underlying mechanisms of action. Using such an approach, with site-moiety mapping, we identified that the candidate synthetic flavonoid protoapigenone WYC02 potentially interacts with PIK3 catalytic subunits. This allowed the present study to focus on the PIK3 signalling pathway. Cell-based assays and an *in vivo* mouse xenograft model indeed confirmed that WYC02 inhibited tumour progression through inhibition of PIK3/AKT1/mTOR signalling and suppressed cell invasion/migration through inhibition of MMP-2/MMP-9.

WYC02-inhibited cervical cancer cell growth and migration/invasion.

The synthetic protoapigenone WYC02 exhibited a number of inhibitory effects on cervical cancer (HeLa) cells. WYC02 inhibition of colony formation, induction of S-G2/M cell cycle arrest (fig 1A–C) and promotion of Hela cell apoptosis (fig 1D–F) were matched by a corresponding suppression of xenograft tumour growth in nude mice (fig. 6A). WYC02 also demonstrated effects on tumour migration and invasion, mediated by suppression of MMP-2/-9-dependent cell invasion/migration (fig. 2). WYC02 may therefore have merit as a potential therapeutic agent in both cervical tumour growth suppression and in inhibition of invasion.

WYC02 increases cervical cancer cell apoptosis via inhibition of the PIK3/AKT1/mTOR pathway.

The PIK3/AKT1 signalling pathway regulates cellular responses and plays a critical role in maintaining the balance between cell survival and apoptosis [15]. Recent studies indicate that activation of the PIK3/AKT pathway by amplification, mutation and translocation occurs on a more frequent basis than in other pathways in patients with cancer [43]. Inhibition of the PIK3 pathway may therefore provide an appropriate target for cancer therapeutic options. Using site-moiety maps to explore binding site, pharmacophore and docking pose similarity, we observed that WYC02 may inhibit the activities of PIK3s (PIK3CA, PIK3CB, PIK3CD and PIK3CG) (fig. 3). Over-expression of PIK3 has been associated with

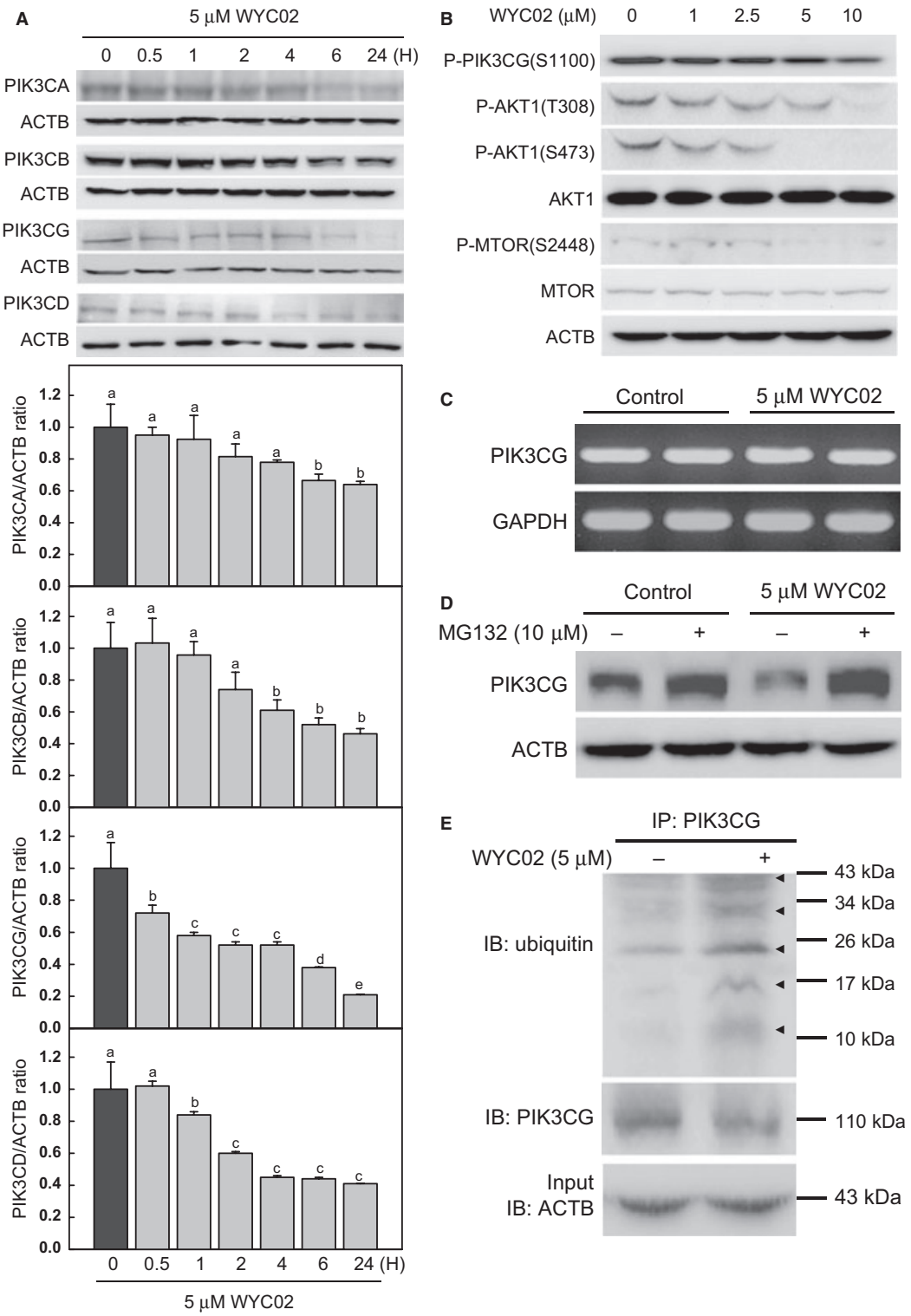

Fig. 4. WYC02 decreased PIK3CG expression and activity through ubiquitination. (A) HeLa cells were treated with 5 μM WYC02 for different time periods and the cell lysates were analysed by immunoblotting for PIK3 catalytic subunits, including PIK3CA, PIK3CB, PIK3CG and PIK3CD. (B) HeLa cells were treated with 1–10 μM WYC02 for 4 hr and cell lysates were analysed by immunoblotting for the activities of PIK3CG and PIK3 downstream molecules AKT1 and MTOR. (C) HeLa cells were treated with WYC02 for 6 hr and PIK3CG RNA level was determined by RT-PCR. (D) HeLa cells were treated with WYC02 for 24 hr and the effect of MG132, an inhibitor of proteasomal protease activity, on the expression of PIK3CG was determined by immunoblotting. (E) HeLa cells were treated with WYC02 for 8 hr and PIK3CG ubiquitination was determined by immunoprecipitation with anti-PI3KCG followed by immunoblotting for PIK3CG and ubiquitin antibodies, respectively. Input ACTB served as an internal control. Arrowheads mark the position of discrete bands, consistent with addition of a different number of ubiquitin moieties (approximately 8.5 kDa per ubiquitin).

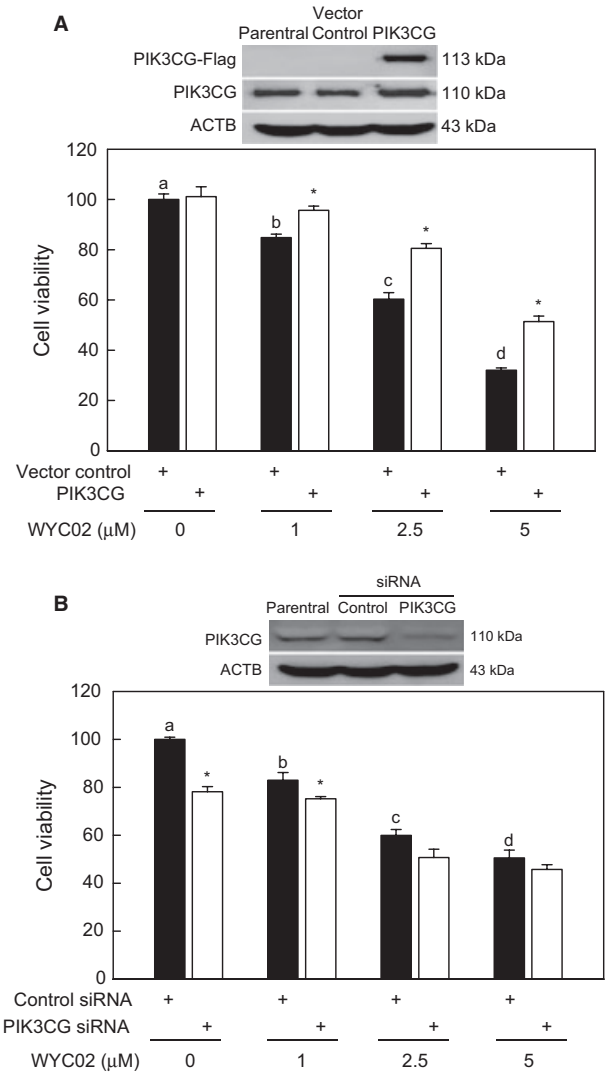

Fig. 5. PIK3CG was involved in the cytotoxic activity of WYC02 on HeLa cells. (A) Immunoblotting analysis of the expression of PIK3CG-Flag in parental, empty vector and PIK3CG-overexpressing HeLa cells. HeLa cells were transfected with PIK3CG-Flag plasmid and then treated with WYC02. (B) Immunoblotting analysis of the expression of PIK3CG in parental, control siRNA- or PIK3CG siRNA-transfected HeLa cells and then treated with WYC02. Cytotoxicity was determined by XTT assay. Each bar represents mean ± S.E.M. (n = 6). *Indicates a significant difference ($p < 0.05$) compared with their respective controls after different doses of WYC02 treatments.

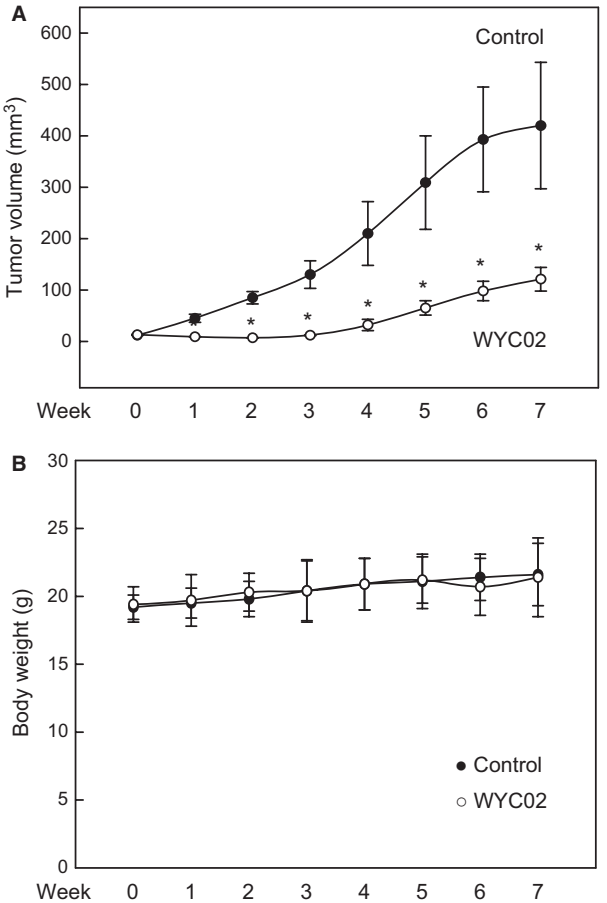

Fig. 6. WYC02 suppressed xenograft tumour growth in nude mice. Nude mice bearing HeLa tumours were treated with vehicle control or 1.09 μg/g (a dose equals to the IC_{50}) WYC02 every 2 days. (A) Tumour volumes were measured per week and data presented as means ± S.E.M. (B) Body-weight was measured per week and data presented as means ± S.E.M. *Indicates a significant difference ($p < 0.05$) when compared with the vehicle control without WYC02 treatment.

tumour stage, grade, lymph node metastasis and poor prognosis in cervical cancer [44,45]. Using site-moiety maps and detection of cellular biological activity in cervical cancer cells, we found that WYC02 inhibited the expression of PIK3CA, PIK3CB, PIK3CD and PIK3CG in a dose-related manner, with the most marked inhibitory effect on PIK3CG (fig. 4A). Decreased PIK3CG activity was accompanied by a decrease in levels of downstream effectors P-AKT1 and mTOR (fig. 4B). The inhibitory effect of WYC02 on cell viability was also reversed by PIK3CG over-expression (fig. 5A). However, this reverse effect was not seen in cervical cancer cells when PI3KCG expression was knockdowned (fig. 5B). It suggests that WYC02 may act by inducing apoptosis in cervical cancer cells, with inhibition of PIK3CG/AKT1/mTOR contributing to the activation of caspases 3, 8 and 9, and PARP cleavage. The precise mechanism by which this occurs is discussed below.

WYC02 targets the PIK3 pathway by promoting PIK3CG ubiquitination.

Distinct from other members in the PIK3 family, PIK3CG is activated by G-protein coupled-receptors and is involved in other processes including inflammation, allergy and thrombosis [46,47]. PIK3CA, PIK3CB and PIK3CD have been implicated as possible oncogenes in human cancers including brain, colon and bladder [48–51]. Emerging data suggest that PIK3CG may also have a role in cancer growth, invasion and metastasis [52,53], suggesting its potential as an oncological therapeutic target.

Proteasome degradation of ubiquitin-targeted proteins is an important mechanism that negatively controls activated signalling pathways [54]. PIK3 degradation via the ubiquitination/

proteasome pathway has previously been shown [39,40]. In this study, we determined whether WYC02 negatively controls PIK3CG signalling via ubiquitination degradation. WYC02 promoted PIK3CG ubiquitination in HeLa cells (fig. 4E), while addition of the proteasome inhibitor MG132 reversed this effect (fig. 4D). We also confirmed that WYC02 had no effect on the mRNA levels of PIK3CG (fig. 4C), further supporting the direct inhibitory effect of WYC02 on protein degradation. Therefore, it was demonstrated that the WYC02-induced decrease in PI3KCG activity was mediated by ubiquination.

Conclusions

In conclusion, using site-moiety maps as an initial approach, we demonstrated that the total synthetic protoapigenone WYC02 suppressed cervical cancer cells *in vitro* and *in vivo* through inhibition of PIK3 signalling pathway. This is the first study to demonstrate the involvement of PIK3CG molecule in cervical tumour progression and that ubiquitination degradation is responsible for the WYC02 inhibitory effect on cancer cell proliferation. Ubiquitination of PIK3CG results in inhibition of AKT1/MTOR activity, leading to activation of caspases 3, 8 and 9, and PARP cleavage, and promotion of apoptosis in cervical cancer cells. WYC02 therefore merits further investigation as a potential therapeutic target in cervical cancer.

Acknowledgements

This manuscript was supported by grants from National Health Research Institutes, Taiwan, ROC (NHRI-EX98, 99,100-9829BI, NHRI-EX102-10212BI, EDPJ99007 and EDPJ100003) to SSY, Department of Health, Taiwan, ROC (DOH101-TD-C-111-002) to MFH and E-DA hospital, Taiwan, ROC (EDAHP99040 and EDAHP101023) to NK.

Conflict of interest

The authors declare no conflicts of interest.

References

1 Wright TC Jr, Kuhn L. Alternative approaches to cervical cancer screening for developing countries. Best Pract Res Clin Obstet Gynaecol 2012;**26**:197–208.
2 Priyadarsini RV, Murugan RS, Maitreyi S, Ramalingam K, Karunagaran D, Nagini S. The flavonoid quercetin induces cell cycle arrest and mitochondria-mediated apoptosis in human cervical cancer (HeLa) cells through p53 induction and NF-kappaB inhibition. Eur J Pharmacol 2010;**649**:84–91.
3 Devita VT, Hellman S, Rosenberg SA (eds). Cancer: Principles and Practice of Oncology, 8th edn. Lippincott Williams & Wilkins, Philadelphia, PA, 2007.
4 Peters WA 3rd, Liu PY, Barrett RJ 2nd, Stock RJ, Monk BJ, Berek JS *et al.* Concurrent chemotherapy and pelvic radiation therapy compared with pelvic radiation therapy alone as adjuvant therapy after radical surgery in high-risk early stage cancer of the cervix. J Clin Oncol 2000;**18**:1606–13.
5 Eifel PJ, Winter K, Morris M, Levenback C, Grigsby PW, Cooper J *et al.* Pelvic irradiation with concurrent chemotherapy versus pelvic and para-aortic irradiation for high-risk cervical cancer: an update of radiation therapy oncology group trial (RTOG). J Clin Oncol 2004;**22**:872–80.
6 Sorbe B, Bohr L, Karlsson L, Bermark B. Combined external and intracavitary irradiation in treatment of advanced cervical carcinomas: predictive factors for local tumor control and early recurrences. Int J Oncol 2010;**36**:371–8.
7 Siddik ZH. Cisplatin: mode of cytotoxic action and molecular basis of resistance. Oncogene 2003;**22**:7265–79.
8 Block G, Patterson B, Subar A. Fruit, vegetables, and cancer prevention: a review of the epidemiological evidence. Nutr Cancer 1992;**18**:1–29.
9 Waladkhani AR, Clemens MR. Effect of dietary phytochemicals on cancer development. Int J Mol Med 1998;**1**:747–53.
10 Li J, Cheng Y, Qu W, Sun Y, Wang Z, Wang H *et al.* Fisetin, a dietary flavonoid, induces cell cycle arrest and apoptosis through activation of p53 and inhibition of NF-kappa B pathways in bladder cancer cells. Basic Clin Pharmacol Toxicol 2011;**108**:84–93.
11 Chen Y, Lu N, Ling Y, Wang L, You Q, Li Z *et al.* LYG-202, a newly synthesized flavonoid, exhibits potent antiangiogenic activity in vitro and in vivo. J Pharmacol Sci 2010;**112**:37–45.
12 He L, Wu Y, Lin L, Wang J, Wu Y, Chen Y *et al.* Hispidulin, a small flavonoid molecule, suppresses the angiogenesis and growth of human pancreatic cancer by targeting vascular endothelial growth factor receptor 2-mediated PI3K/Akt/mTOR signaling pathway. Cancer Sci 2011;**102**:219–25.
13 Kim JH, Kang JW, Kim MS, Bak Y, Park YS, Jung KY *et al.* The apoptotic effects of the flavonoid N101–2 in human cervical cancer cells. Toxicol In Vitro 2012;**26**:67–73.
14 Lee YC, Cheng TH, Lee JS, Chen JH, Liao YC, Fong Y *et al.* Nobiletin, a citrus flavonoid, suppresses invasion and migration involving FAK/PI3K/Akt and small GTPase signals in human gastric adenocarcinoma AGS cells. Mol Cell Biochem 2011;**347**:103–15.
15 Fagone P, Donia M, Mangano K, Quattrocchi C, Mammana S, Coco M *et al.* Comparative study of rapamycin and temsirolimus demonstrates superimposable antitumour potency on prostate cancer cells. Basic Clin Pharmacol Toxicol 2013;**112**:63–9.
16 Błajecka K, Borgström A, Arcaro A. Phosphatidylinositol 3-kinase isoforms as novel drug targets. Curr Drug Targets 2011;**12**:1056–81.
17 Costa C, Martin-Conte EL, Hirsch E. Phosphoinositide 3-kinase p110γ in immunity. IUBMB Life 2011;**63**:707–13.
18 Hawkins PT, Anderson KE, Davidson K, Stephens LR. Signalling through Class I PI3Ks in mammalian cells. Biochem Soc Trans 2006;**34**(Pt 5):647–62.
19 Kramer B, Rarey M, Lengauer T. Evaluation of the FLEXX incremental construction algorithm for protein-ligand docking. Proteins 1999;**37**:228–41.
20 Morris GM, Goodsell DS, Huey R, Olson AJ. Distributed automated docking of flexible ligands to proteins: parallel applications of AutoDock 2.4. J Comput Aided Mol Des 1996;**10**:293–304.
21 Yang JM, Chen CC. GEMDOCK: a generic evolutionary method for molecular docking. Proteins 2004;**55**:288–304.
22 Hsu KC, Chen YF, Lin SR, Yang JM. iGEMDOCK: a graphical environment of enhancing GEMDOCK using pharmacological interactions and post-screening analysis. BMC Bioinformatics 2011;**1**:S33.
23 Yang JM, Shen TW. A pharmacophore-based evolutionary approach for screening selective estrogen receptor modulators. Proteins 2005;**59**:205–20.
24 Lin AS, Nakagawa-Goto K, Chang FR, Yu D, Morris-Natschke SL, Wu CC *et al.* First total synthesis of protoapigenone and its analogues as potent cytotoxic agents. J Med Chem 2007;**50**:3921–7.
25 Jiang Y, Rom WN, Yie TA, Chi CX, Tchou-Wong KM. Induction of tumor suppression and glandular differentiation of A549 lung carcinoma cells by dominant-negative IGF-I receptor. Oncogene 1999;**18**:6071–7.

26 Chen YJ, Hung CM, Kay N, Chen CC, Kao YH, Yuan SS. Progesterone receptor is involved in 2,3,7,8-tetrachlorodibenzo-p-dioxin-stimulated breast cancer cells proliferation. Cancer Lett 2012;**319**:223–31.
27 Chang HL, Wu YC, Su JH, Yeh YT, Yuan SS. Protoapigenone, a novel flavonoid, induces apoptosis in human prostate cancer cells through activation of p38 mitogen-activated protein kinase and c-Jun NH2-terminal kinase 1/2. J Pharmacol Exp Ther 2008;**325**:841–9.
28 Kim SW, Zhang HZ, Guo L, Kim JM, Kim MH. Amniotic mesenchymal stem cells enhance wound healing in diabetic NOD/SCID mice through high angiogenic and engraftment capabilities. PLoS ONE 2012;**7**:e41105.
29 Zhang L, Wang N, Zhou S, Ye W, Jing G, Zhang M. Propofol induces proliferation and invasion of gallbladder cancer cells through activation of Nrf2. J Exp Clin Cancer Res 2012;**31**:66.
30 Ke FC, Chuang LC, Lee MT, Chen YJ, Lin SW, Wang PS *et al.* The modulatory role of transforming growth factor beta1 and androstenedione on follicle-stimulating hormone-induced gelatinase secretion and steroidogenesis in rat granulosa cells. Biol Reprod 2004;**70**:1292–8.
31 Krymskaya VP, Ammit AJ, Hoffman RK, Eszterhas AJ, Panettieri RA Jr. Activation of class IA PI3K stimulates DNA synthesis in human airway smooth muscle cells. Am J Physiol Lung Cell Mol Physiol 2001;**280**:L1009–18.
32 Yeh YT, Ou-Yang F, Chen IF, Yang SF, Wang YY, Chuang HY *et al.* STAT3 ser727 phosphorylation and its association with negative oestrogen receptor status in breast infiltrating ductal carcinoma. Int J Cancer 2006;**118**:2943–7.
33 Watanabe H. Extracellular matrix–regulation of cancer invasion and metastasis. Gan To Kagaku Ryoho 2010;**37**:2058–61.
34 Roomi MW, Monterrey JC, Kalinovsky T, Rath M, Niedzwiecki A. In vitro modulation of MMP-2 and MMP-9 in human cervical and ovarian cancer cell lines by cytokines, inducers and inhibitors. Oncol Rep 2010;**23**:605–14.
35 Ishii K, Tanaka S, Kagami K, Henmi K, Toyoda H, Kaise T *et al.* Effects of naturally occurring polymethyoxyflavonoids on cell growth, p-glycoprotein function, cell cycle, and apoptosis of daunorubicin-resistant T lymphoblastoid leukemia cells. Cancer Invest 2010;**28**:220–9.
36 Luo G, Zeng Y, Zhu L, Zhang YX, Zhou LM. Inhibition effect and its mechanism of nobiletin on proliferation of lung cancer cells. Sichuan Da Xue Xue Bao Yi Xue Ban 2009;**40**:449–53.
37 Hernando E, Charytonowicz E, Dudas ME, Menendez S, Matushansky I, Mills J *et al.* The AKT-mTOR pathway plays a critical role in the development of leiomyosarcomas. Nat Med 2007;**13**:748–53.
38 Hunter T. Signaling–2000 and beyond. Cell 2000;**100**:113–27.
39 Lu Z, Hunter T. Degradation of activated protein kinases by ubiquitination. Annu Rev Biochem 2009;**78**:435–75.
40 Guenou H, Kaabeche K, Dufour C, Miraoui H, Marie PJ. Down-regulation of ubiquitin ligase Cbl induced by twist haploinsufficiency in Saethre-Chotzen syndrome results in increased PI3K/Akt signaling and osteoblast proliferation. Am J Pathol 2006;**169**:1303–11.
41 da Rocha AB, Lopes RM, Schwartsmann G. Natural products in anticancer therapy. Curr Opin Pharmacol 2001;**1**:364–9.
42 Chung KS, Choi JH, Back NI, Choi MS, Kang EK, Chung HG *et al.* Eupafolin, a flavonoid isolated from Artemisia princeps, induced apoptosis in human cervical adenocarcinoma HeLa cells. Mol Nutr Food Res 2010;**54**:1318–28.
43 Hennessy BT, Smith DL, Ram PT, Lu Y, Mills GB. Exploiting the PI3K/AKT pathway for cancer drug discovery. Nat Rev Drug Discov 2005;**4**:988–1004.
44 Schwarz JK, Payton JE, Rashmi R, Xiang T, Jia Y, Huettner P *et al.* Pathway-specific analysis of gene expression data identifies the PI3K/Akt pathway as a novel therapeutic target in cervical cancer. Clin Cancer Res 2012;**18**:1464–71.
45 Yao TT, Dai YZ, Li SZ. Expression and clinical significance of phosphatidylinositol 3-kinase and protein kinase B in cervical carcinoma. Ai Zheng 2008;**27**:525–30.
46 Hirsch E, Lembo G, Montrucchio G, Rommel C, Costa C, Barberis L. Signaling through PI3Kgamma: a common platform for leukocyte, platelet and cardiovascular stress sensing. Thromb Haemost 2006;**95**:29–35.
47 Venable JD, Ameriks MK, Blevitt JM, Thurmond RL, Fung-Leung WP. Phosphoinositide 3-kinase gamma (PI3Kgamma) inhibitors for the treatment of inflammation and autoimmune disease. Recent Pat Inflamm Allergy Drug Discov 2010;**4**:1–15.
48 Knobbe CB, Reifenberger G. Genetic alterations and aberrant expression of genes related to the phosphatidyl-inositol-3′-kinase/protein kinase B (Akt) signal transduction pathway in glioblastomas. Brain Pathol 2003;**13**:507–18.
49 Song Z, Song M, Lee DY, Liu Y, Deaciuc IV, McClain CJ. Silymarin prevents palmitate-induced lipotoxicity in HepG2 cells: involvement of maintenance of Akt kinase activation. Basic Clin Pharmacol Toxicol 2007;**101**:262–8.
50 Denley A, Kang S, Karst U, Vogt PK. Oncogenic signaling of class I PI3K isoforms. Oncogene 2008;**27**:2561–74.
51 Denley A, Gymnopoulos M, Kang S, Mitchell C, Vogt PK. Requirement of phosphatidylinositol(3,4,5)trisphosphate in phosphatidylinositol 3-kinase-induced oncogenic transformation. Mol Cancer Res 2009;**7**:1132–8.
52 Schmid MC, Avraamides CJ, Dippold HC, Franco I, Foubert P, Ellies LG *et al.* Receptor tyrosine kinases and TLR/IL1Rs unexpectedly activate myeloid cell PI3kγ, a single convergent point promoting tumor inflammation and progression. Cancer Cell 2011;**19**:715–27.
53 Semba S, Itoh N, Ito M, Youssef EM, Harada M, Moriya T *et al.* Down-regulation of PIK3CG, a catalytic subunit of phosphatidylinositol 3-OH kinase, by CpG hypermethylation in human colorectal carcinoma. Clin Cancer Res 2002;**8**:3824–31.
54 Roos-Mattjus P, Sistonen L. The ubiquitin-proteasome pathway. Ann Med 2004;**36**:285–95.

Supporting Information

Additional Supporting Information may be found in the online version of this article:

Fig. S1. WYC02 at 2 μM had no significant cytotoxicity on HeLa cells at 100% confluence. Cells were treated with indicated concentrations of WYC02 for 24 hr. (A) Cytotoxicity was determined by XTT assay. (B) The whole cell lysates were analysed by immunoblotting analysis.

Fig. S2. Haematoxylin and eosin staining of tissues from mouse organs. The tissues from mouse organs, with or without WYC02 treatment, were fixed with 10% buffered formalin overnight and then dehydrated and coated with wax. Tissue sections were sliced to 3 μm in thickness and the slides were counter-stained with haematoxylin and eosin. The pictures were captured by Nikon Eclipse-80i microscope (Tokyo, Japan). Original magnification was ×200. Bar represents 200 μm. Arrow indicates cervical epithelial cells.

Fig. S3. Tumour samples were analysed by immunohistochemistry for the expression of PIK3CA, PIK3CB, PIK3CG and PIK3CD. Original magnification was ×100. Bar represents 100 μm.

Table S1. Complete blood count and biochemical profile for the nude mice after WYCO2 treatment for 7 weeks.